



HAL
open science

Investigation of the structure of iron oxide nanoparticle assemblies in order to optimize the sensitivity of surface plasmon resonance-based sensors

Mathias Dolci, Jean-François Bryche, Julien Moreau, Cédric Leuvrey, Sylvie Begin-Colin, Grégory Barbillon, Benoit Pichon

► To cite this version:

Mathias Dolci, Jean-François Bryche, Julien Moreau, Cédric Leuvrey, Sylvie Begin-Colin, et al.. Investigation of the structure of iron oxide nanoparticle assemblies in order to optimize the sensitivity of surface plasmon resonance-based sensors. *Applied Surface Science*, 2020, 527, pp.146773. 10.1016/j.apsusc.2020.146773 . hal-03350920

HAL Id: hal-03350920

<https://hal-iogs.archives-ouvertes.fr/hal-03350920>

Submitted on 22 Aug 2022

HAL is a multi-disciplinary open access archive for the deposit and dissemination of scientific research documents, whether they are published or not. The documents may come from teaching and research institutions in France or abroad, or from public or private research centers.

L'archive ouverte pluridisciplinaire **HAL**, est destinée au dépôt et à la diffusion de documents scientifiques de niveau recherche, publiés ou non, émanant des établissements d'enseignement et de recherche français ou étrangers, des laboratoires publics ou privés.



Distributed under a Creative Commons Attribution - NonCommercial 4.0 International License

Investigation of the Structure of Iron Oxide Nanoparticle Assemblies in Order to Optimize the Sensitivity of Surface Plasmon Resonance-Based Sensors

Mathias Dolci,^{*,1} Jean-François Bryche,^{2,3} Julien Moreau,³ Cédric Leuvrey,¹ Sylvie Begin-Colin,¹ Grégory Barbillon,^{*,4} Benoit P. Pichon^{*,1,5}

¹ Université de Strasbourg, CNRS, Institut de Physique et Chimie des Matériaux de Strasbourg, UMR 7504, F-67000 Strasbourg, France

² Centre de Nanosciences et de Nanotechnologies, CNRS, Université Paris Sud, Université Paris Saclay, C2N-Orsay, 91405 Orsay, France

³ Laboratoire Charles Fabry, Institut d'Optique Graduate School, Université Paris Sud, Université Paris Saclay, 91127 Palaiseau, France

⁴ EPF-Ecole d'Ingénieurs, 3 bis rue Lakanal, 92330 Sceaux, France

⁵ Institut Universitaire de France, 1 rue Descartes, 75231 Paris Cedex 05

Corresponding Authors

E-mail : benoit.pichon@unistra.fr, mathias.dolci@gmail.com, gregory.barbillon@epf.fr

Tel: 0033 (0)3 88 10 71 33, Fax: 0033 (0)3 88 10 72 47

Abstract

Surface plasmon resonance (SPR) biosensors based on metal thin films are very attractive for detection of biomolecules. Nanoparticle assemblies were recently demonstrated to significantly enhance sensitivity. Here, we show that the fine control of the structure of nanoparticle assemblies is critical to optimize the sensitivity. Iron oxide ($\text{Fe}_{3-\delta}\text{O}_4$) nanoparticles were assembled onto a gold thin film by performing the Copper Catalyzed Alkyne-Azide cycloaddition (CuAAC) “click” reaction. A biotin derivative was grafted by CuAAC at the surface of nanoparticle assemblies in order to detect streptavidin (SA). The fine control of the size and of the density of nanoparticles allowed tuning the surface plasmon waves at the surface of the gold thin film in order to optimize the response of the sensors. The accessibility of biotin at the nanoparticle surface to SA was also investigated as a function of the interparticle distance. We show that the interplay between the volume fraction of iron oxide and the accessibility of biotin at the nanoparticle surface is critical to enhance the sensitivity of SPR sensors.

Keywords

Nanoparticle assembly, biosensor, surface plasmon resonance, click chemistry

1. Introduction

The surface plasmon resonance (SPR) phenomenon results from the interaction between an electromagnetic wave and the collective oscillation of electrons at a metal/dielectric interface.[1] A slight variation of the refractive index at this interface shifts the position of the resonance of surface plasmon wavelength, which can be directly monitored through the measurement of the SPR reflectivity signal.[2] Therefore, this technique is perfectly suited for the monitoring of biomolecular recognition processes. SPR biosensors became a powerful tool for the detection of target molecules in various domains such as biomedicine, food safety and security.[3] Despite their low limit of detection (down to 10^{-7} RIU - refractive index units), the main limits come from the lack of sensitivity to detect small molecules (below hundreds of Daltons).[4,5] Different strategies have been employed to increase the sensitivity of SPR biosensors such as prism coupling[6,7], diffraction on periodic metallic gratings[8–10] and interferometric methods.[11–14] Among these techniques, the deposition of a thin dielectric layer onto a gold thin film surface showed an improvement on the SPR biosensing performances.[15–19] Lahav et al. reported on nearly-guided wave SPR (NGWSPR) which takes advantage of a thin dielectric layer that guides optical waves in transverse electric modes. The sensitivity of a gold thin film was enhanced by one magnitude order in comparison with classical SPR.[20] Dielectric materials such as a thin layer of silicon oxide (SiO_x , < 60 nm, refractive index of 1.48) was also be used as a protective layer.[21] The increase of the SiO_x film thickness resulted in the shift of the SPR signal to longer wavelengths. Furthermore, the surface of such a dielectric layer was functionalized by biomolecules in order to detect analytes.[16,21,22] Hence, the deposition of nanostructured dielectric materials with high refractive index at the surface of the metal thin films is a very promising strategy to enhance the sensitivity of SPR sensors. Moreover, the topography of non-planar surfaces allows higher binding capacity of the bioreceptors with target molecules, thus contributing to the enhancement of the sensitivity. With this aim, the quantity of bioreceptors and their availability (no steric hindrance) are critical parameters.[23] Although lithography techniques allow the fabrication of various geometries, the effective cost and the restricted surface of such patterns limit the interest of such approaches.

An alternative is the preparation of a nanoparticle assembly onto a metal thin film that allows the fine-tuning of the surface geometry and chemistry.[24][25] Our recent work showed that the increase of the nanoparticle density onto a gold thin film resulted in the significant enhancement of the sensitivity of the SPR signal, i.e. a larger spectral shift, after the adsorption of analytes.[26] Such a behavior was ascribed to the presence of iron oxide ($\text{Fe}_{3-\delta}\text{O}_4$) nanoparticles which display a high refractive index of 2.42, responsible of the enhancement of the sensitivity factor.

Nanoparticle assemblies present the great advantage that their structure can be easily tuned as a function of the nanoparticle size and density. Furthermore, the interparticle distance allows to control the number of bio receptors available at the nanoparticle surface (Fig. 1). In this context, we investigated further the way that nanoparticle assemblies enhance the sensitivity of SPR sensors based on a gold thin film. We studied the interplay between the volume fraction of nanoparticles and the interparticle distance which favors the sensitivity factor and the number of analytes to detect. Nanoparticles with different sizes were assembled by performing the Copper Catalyzed Alkyne-Azide cycloaddition (CuAAC)

“click” reaction for different times in order to modulate the volume fraction of iron oxide at the surface of gold thin film. Biotin was grafted at the surface of nanoparticles in order to detect streptavidin.

2. Experimental section

Materials and products. Iron II stearate (Strem Chemicals), dioctylether (99%, Aldrich), oleic acid (99%, Alfa Aesar), 10-undecyn-1-ol (96%, Alfa Aesar), triethylamine (99%, Acros Organics), N-[2-[2-[2-(2-azidoethoxy)ethoxy]ethoxy]ethyl]biotinamide (>95%, TCI), 1-(3-dimethylaminopropyl)-3-ethylcarbodiimide hypochloride (>98%, TCI), bromotris(phenylphosphine) copper I (98%, Aldrich).

2.1. Molecule synthesis.

2.1.a. Synthesis of (11-Undec-1-ynyl)thiol. (11-Undec-1-ynyl)thiol was synthesized from (11-undec-1-ynyl)thioacetate, which has been synthesized following the synthesis pathway reported previously.^[10] Then, 300 mg of (11-undec-1-ynyl)thioacetate were dissolved in 20 mL of methanol. The solution was degassed thoroughly and backfilled with N₂. One milliliter of concentrated HCl was added dropwise, and the entire mixture was refluxed under N₂ atm for 5h. The reaction was then stopped by adding 20 mL of ice-cold water. The product was extracted twice with diethyl ether (20 mL), and the organic phase was washed twice with water (20 mL) and dried over MgSO₄. Rotary evaporation yielded a yellow oil. ¹H NMR (CDCl₃, 400 MHz): 2.52 (q, J = 7.3 Hz, 2H); 2.18 (dt, J = 6.8 and 2.6 Hz, 2H); 1.94 (t, J = 2.6 Hz, 1H); 1.61 (m, 4H); 1.22–1.41 (m, 11H). ¹³C NMR (CDCl₃, 100 MHz): 85.6 (C terminal C–H); 67.9 (C alkyne); 39.1 (CH₂–SH); 30.2–28.4 (6 CH₂); 22.6 (CH₂); 18.3 (CH₂); 14.0 (CH₂).

2.1.b. Synthesis of Alkynated Biotin. Alkynated biotin synthesis was inspired by Cao *et al.*^[27] 200 mg of biotin and 102 mg of NHS were dissolved in 15 mL of DMF. 184 mg of EDC HCl was added and the resultant solution was stirred at room temperature for 24h under argon. The solution was then evaporating under vacuum and a white solid product was obtained. 145 mg of the white product was added to 115 μL of triethylamine and 55 μL of propargylamine in 8 mL of DMF. The solution was stirred for 24h at room temperature under argon, concentrated and purified by column chromatography to give alkynated biotin as a white solid. ¹H NMR (DMSO, d₆) 1.29-1.33 (m, 2H), 1.44-1.51 (m, 2H), 2.07-2.10 (d, J = 7.5 Hz, 2H), 2.57-2.59 (d, J = 13.0 Hz, 1H), 2.81-2.84 (dd, J₁ = 4.5 Hz, J₂ = 5.0 Hz, 1H), 3.04-3.09 (m, 2H), 4.13 (m, 1H), 4.29-4.31 (m, 1H), 6.31 (s, 1H), 6.36 (s, 1H), 8.17 (s, 1H).

2.2. Preparation of azide-terminated magnetite nanoparticles (Fe_{3-δ}O₄@N₃). 10 nm-sized Fe_{3-δ}O₄ nanoparticles have been synthesized following the exact procedure reported earlier.^[10] Iron oxide nanoparticles were synthesized by pouring 1.38 g (2.22 mmol) of Fe(stearate)₂, 1.254 g (4.44 mmol) of oleic acid, and 20 mL of dioctylether in a two necked round bottom flask. After stirring at 110°C for 60 min until a clear solution was obtained, the reaction medium was then heated to boiling temperature (≈ 287°C) with a heating rate of 5°C/min and kept at this temperature for 120 min under air. The resultant black solution was then cooled at room temperature. 5 nm-sized nanoparticles have been obtained without adding oleic acid in the mixture. 20 nm-sized nanoparticles have been obtained by replacing the dioctylether by squalane. The nanoparticles were precipitated by the addition of an acetone excess and washed several times by a mixture of chloroform/acetone (1/4) followed by centrifugation (14000 rpm, 10 min). Nanoparticles were then easily dispersed in THF. Further, a solution of (12-azidododecyl) phosphonic acid (AP12N₃) (15 mg dissolved in THF (10 mL)) was added to 10 mL of the nanoparticle

suspension and stirred for 24h at room temperature. Free molecules were removed by ultrafiltration (using a 30 kDa membrane, Millipore) in 60 mL of THF and allowed the preparation of a Fe_{3-δ}O₄@N₃ suspension in THF (1 mg/mL).

2.3. Nanoparticle Assembling. A gold film with a thickness of 30 nm was evaporated onto a BK7 glass substrate after an evaporation of a 3-nm thick titanium adhesion layer. The assembling of Fe₃O₄@N₃ nanoparticles onto alkyne-terminated gold substrate (SAM-CC) was performed following the exact procedure reported earlier.[28] First, SAM-CC were prepared by immersion of a gold substrates for 24h in an 10-mM ethanolic solution of (11-Undec-1-ynyl)thiol after activation by a plasma cleaner (5 minAr/H₂). Fe₃O₄@N₃ were assembled onto SAM-CC by performing copper catalyzed azido-alkyne (CuAAC) “click” reaction. A SAM-CC (5 × 5 mm²) was immersed in 5 mL of a solution of Fe₃O₄@N₃ in THF. Then, 0.5 mL (3.70 mmol) of triethylamine and 6.5 mg (6.7×10⁻³ mmol) of CuBr(PPh₃)₃ were added. The reaction was performed under reflux in 48 hours. Substrates were extensively washed with THF and dried under a nitrogen stream.

2.4. Surface modification by Alkynated biotin, azide biotin and Streptavidin adsorption. The click reaction follows the same procedure than for the NPs assembly. 10 mg of alkynated biotin, 6.5 mg of CuBr(PPh₃)₃ and 0.5 mL of Et₃N were stirred in 5 mL of THF in a 50 mL reactor. The reaction was performed under microwave irradiation (30 W/120°C) in 30 min. The substrates were then rinsed and ultrasonicated for 1 min in THF before being dry under air stream. Samples were then immersed in a solution of Streptavidin in milliQ water (100 µg/mL) for 30 min. Substrates were extensively washed with deionized water then dried under an air stream.

2.5. Sample characterization. Transmission electron microscopy (TEM), high resolution TEM (HRTEM), and electron diffraction (ED) were performed with a TOPCON model 002B TEM, operating at 200 kV, with a point-to-point resolution of 0.18 nm. Transmission electron microscopy (TEM) has been performed on a JEOL ARF200F microscope operating at 200 kV. The size distribution was calculated from the size measurement of more than 100 nanoparticles by using the Image J software. Granulometry measurements were performed using a MALVERN (nano ZS) apparatus. Fourier transform infrared (FTIR) spectroscopy was performed using Perkin Elmer Spectrum Two spectrophotometer in the energy range 4000–400 cm⁻¹. Scanning electron microscopy (SEM) was performed using a Zeiss gemini SEM 500 microscope equipped with a field emission gun (SEM-FEG) operating at an accelerating voltage of 1 kV. The nanoparticle density was calculated manually from SEM micrographs that were recorded on, at least, four different regions of the sample. SEM micrographs corresponding to a magnification of 50 000 times. Each micrograph was divided in four equal regions (2.2 µm²) from which nanoparticles were counted manually.

3. Results and discussion

3.1. Preparation of nanoparticle assemblies with tunable structures

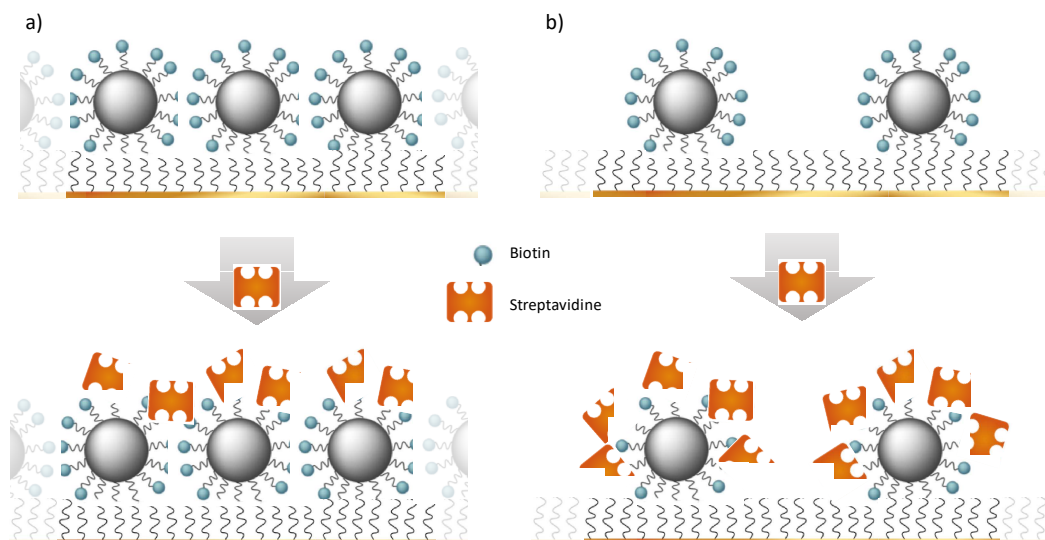


Fig. 1. Illustration of the sensor process. Biotin groups grafted at the surface of nanoparticles assembled onto a gold thin film allowed the adsorption of streptavidine through biomolecular recognition. The number of adsorbed streptavidin depends on the availability of biotin groups at the nanoparticle surface. a) Tight packed nanoparticles. b) Large interparticle distance.

Iron oxide nanoparticles were synthesized by performing the thermal decomposition technique as reported previously.[29] Specific parameters such as solvent and stabilizing agent were modulated in order to produce nanoparticles with well-defined spherical shape and narrow size distributions centered to 5.7 ± 0.9 nm, 10.1 ± 1.1 nm and 21.9 ± 1.6 nm (see supporting information, Fig. S1). Nanoparticles were named NP6, NP10 and NP22, respectively, in agreement with their mean size. Highly stable colloidal suspensions were obtained thanks to oleic acid molecules adsorbed at their surface.

Each nanoparticle type was further assembled onto a gold thin films (30-nm thick) by performing the copper alkyne-azide catalyzed cycloaddition (CuAAC) “click” reaction as we reported earlier.[30] This approach is very attractive because of its reliability as well as of the robustness of nanoparticle assembly. With this aim, oleic acid was replaced by 1-(12-azidododecyl) phosphonic acid (AP12N₃) at the nanoparticle surface and 11-mercapto-undecyn molecules were self-assembled onto the gold thin film. The CuAAC reaction was performed for 48 hours in order to assemble azide-terminated nanoparticles onto the gold thin film through the irreversible formation of triazole bonds. Nanoparticles assemblies were denoted as NP6_{48h}, NP10_{48h} and NP22_{48h}. The CuAAC reaction was also performed for 8h in order to create sample NP6_{8h}. SEM was performed to determine the spatial arrangement of nanoparticles onto the gold thin film (Fig. 2). The density of nanoparticles was calculated manually from SEM micrographs and normalized as a function of the maximum theoretical value corresponding to the hexagonal close packing arrangement. The samples exhibit monolayer of nanoparticles with high density for NP22_{48h}

(1700 ± 140 NPs/ μm^2) and NP10_{48h} (3550 ± 325 NPs/ μm^2) which is promoted by a dipolar interaction assisted assembly process that we reported recently.[31] In contrast, the nanoparticle densities calculated for NP6_{48h} (4220 ± 395 NPs/ μm^2) and NP6_{8h} (2000 ± 95 NPs/ μm^2) are much lower than maximum theoretical density ($12\ 300$ NPs/ μm^2) because of weak dipolar interactions. Furthermore, AFM height images confirmed that nanoparticle are assembled in monolayers (see Fig. S2). The maximum value of the height profile cross-sections agree with the nanoparticle size. As expected, the average roughness increases with the nanoparticle size.

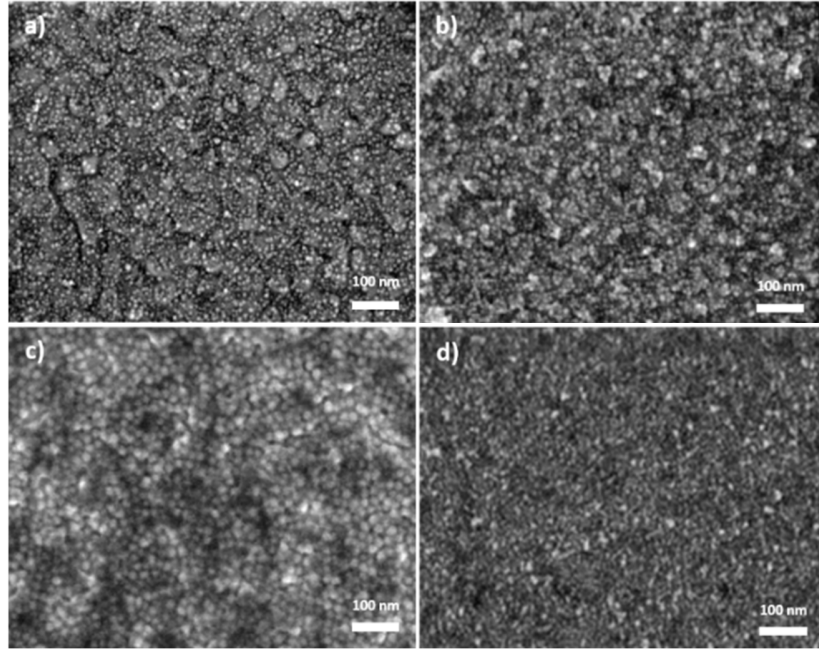


Fig. 2. SEM images of nanoparticle assemblies obtained after different reaction times. a) NP6_{48h}, b) NP10_{48h}, c) NP22_{48h}, d) NP6_{8h}.

The aim of this work is to monitor the plasmon resonance signal as a function of the variation of the refractive index of the dielectric medium in the vicinity of the gold thin film. We considered the volume fraction of iron oxide ($V_{\text{Fe}_{3-\delta}\text{O}_4}$) which refers to both variation of density and size of nanoparticles. It is defined as the volume occupied by the nanoparticle (V_{NP}) in the volume of a $1\ \mu\text{m}^2$ layer with a thickness corresponding to the largest nanoparticles (21.9 nm) (V_{Tot}):

$$V_{\text{Fe}_{3-\delta}\text{O}_4} = \frac{V_{\text{NP}}}{V_{\text{Tot}}} = \frac{\left[\frac{4}{3}\pi\left(\frac{D}{2}\right)^3\right]*d}{10^6*21.9} \quad (1)$$

with D , the nanoparticle diameter and d the density of nanoparticle per μm^2 . The $V_{\text{Fe}_{3-\delta}\text{O}_4}$ and the density of each nanoparticle assembly are given in table 1.

Table 1. Density of nanoparticles and the volume fraction of iron oxide corresponding to assemblies prepared onto gold thin films.

	NP6 _{8h}	NP6 _{48h}	NP10 _{48h}	NP22 _{48h}
Density (NP/ μm^2)	2200	4220	3550	1700
Volume fraction (%)	0.9	1.9	8.7	42.7

Biotin groups were grafted at the surface of nanoparticle assemblies in order to detect streptavidin. The CuAAC “click” reaction was performed between alkyated-modified biotin and azide-terminated nanoparticle assembly as we reported earlier.[26] The presence of biotin groups was confirmed by the decrease of hydrophobicity, measured by contact angle from 100° to 52° before and after functionalization with biotin groups, respectively (data not shown). Moreover, the disappearance of the $\nu(\text{N}_3)$ band at 2100 cm^{-1} in PM-IRRAS spectra confirmed the total grafting of the biotin derivative (see SI).[32]

3.2. Influence of the structure of nanoparticle assemblies on the detection of SA

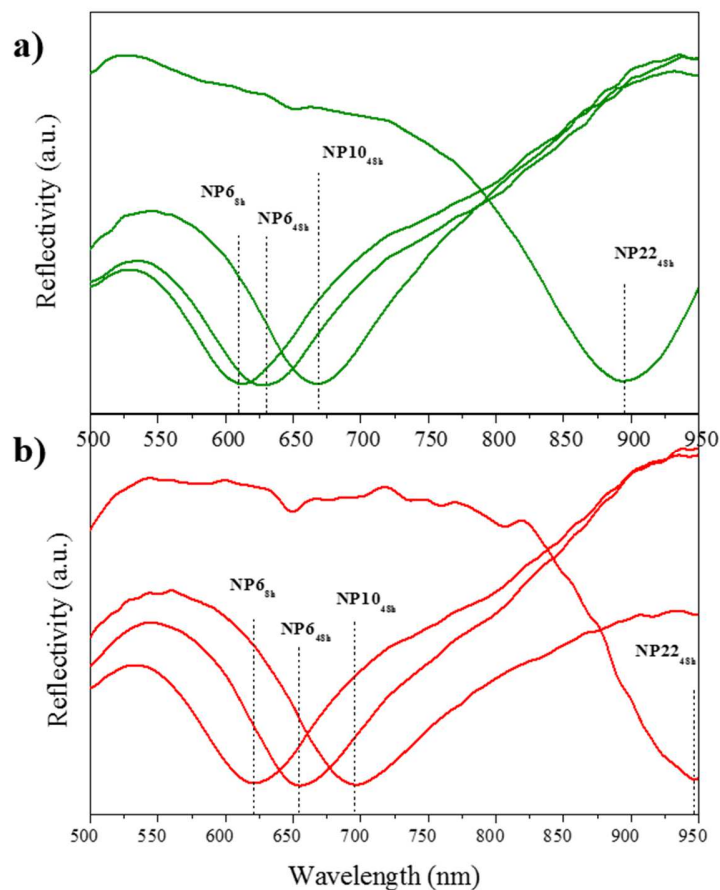


Fig. 3. SPR measurements performed on gold thin films covered by different nanoparticle assemblies a) before and b) after SA adsorption.

The SPR measurements were carried out on gold thin films covered by nanoparticle assemblies by exciting the surface plasmon with an attenuated total reflection (ATR) setup in the Kretschmann configuration. The wavelength of the incident light was varied from 600 nm to 950 nm while maintaining the incident angle to 74°. Measurements were performed first on gold thin films covered by biotin terminated nanoparticle assemblies, e.g. before exposition to streptavidin (Fig. 2a). The position of the minimum of reflectivity shifted to higher wavelengths when the volume fraction of iron oxide ($V_{\text{Fe}_3\text{-}\delta\text{O}_4}$) increased. It linearly increased from 611 nm, without nanoparticles, to 893 nm with the highest volume fraction of iron oxide for NP22_{48h} (Fig. 3, Table 2). These results are consistent with our previous work on the increase of the density of 10 nm sized nanoparticles assembled onto a gold thin film.[24]

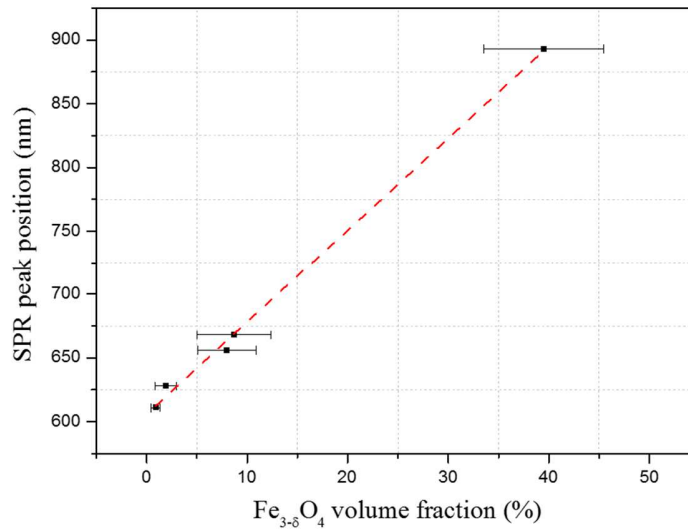


Fig. 4. SPR peak position plotted as a function of the iron oxide volume fraction.

After dipping in a SA aqueous solution of 100 µg/mL, the SPR peak also shifted to higher wavelengths for each sample (Fig. 3b). It agrees with the adsorption of SA at the surface of biotin terminated nanoparticle assemblies as we reported recently.[26] The wavelength shifts ($\Delta\lambda$) also increased significantly and linearly with the iron oxide volume fraction (Table 2, Fig. 4). It is the lowest for NP6_{8h} (11 nm) and the largest for NP22_{48h} (53 nm). $\Delta\lambda$ directly depends on several parameters as shown by the Campbell equation:[33]

$$\Delta\lambda = m\Delta n \left[1 - e^{-\frac{2t}{l_d}} \right] \quad (2)$$

where m is the sensitivity factor, Δn is the local change in the refractive index ($\Delta n = n_{\text{adsorbate}} - n_{\text{water}}$, with $n_{\text{adsorbate}} = n_{\text{streptavidin}} = 1.57$ and $n_{\text{water}} = 1.33$), l_d is the characteristic evanescent electric field decay length, and t is the effective adsorbate layer thickness.

The enhancement of the SPR shift depends directly of the increase of m and of the decrease of l_d . In the case of spectral interrogation, the presence of high refractive index nanoparticles shifts the resonance peaks to higher wavelengths (Fig. 3) and results in higher m and l_d . An analytical study showed that m predominates over l_d (Fig. S5). Although both parameters have opposite effects on $\Delta\lambda$, the SPR response

between 600 nm and 900 nm increases about a factor 1.8. However, it is not sufficient to explain the 5-fold enhancement of the SPR response in the case of NP22_{48h} which corresponds to the highest volume of iron oxide.

To understand the origin of the sensitivity enhancement, we calculated the theoretical maximum amount of SA/ μm^2 that can be adsorbed onto nanoparticles. Knowing the projected area of streptavidin (20.25 nm²),^[34] the accessible area per nanoparticle can be calculated as a function of their size and of the interparticle distance. The number of SA adsorbed per nanoparticle increases continuously with the nanoparticle density (Fig. 5). Nevertheless, the amount of SA is the highest for an interparticle distance of about 4.6 nm, whatever the nanoparticle size. One may expect a value of 9 nm corresponding to the size of two SA, each adsorbed on the side of two neighboring nanoparticles. However, our calculations (Fig. S6a) showed that the number of SA adsorbed at the nanoparticle surface increased much less significantly for distances larger than 4.6 nm. Considering the finite size of the gold thin film, the nanoparticle density decreases markedly when the interparticle distance increases (Fig. S6c). Therefore, the interplay between the interparticle distance and the finite size of substrate resulted in an optimized interparticle distance of 4.6 nm to get the highest theoretical density of SA at the surface of nanoparticles assembled onto a gold thin film. Larger nanoparticles also favor the adsorption of SA because they allow a larger surface area for biotin per nanoparticle. Although the finite surface of the gold substrate, the topography resulting from assemblies of the largest nanoparticles favors the number of available biotin groups.^[31]

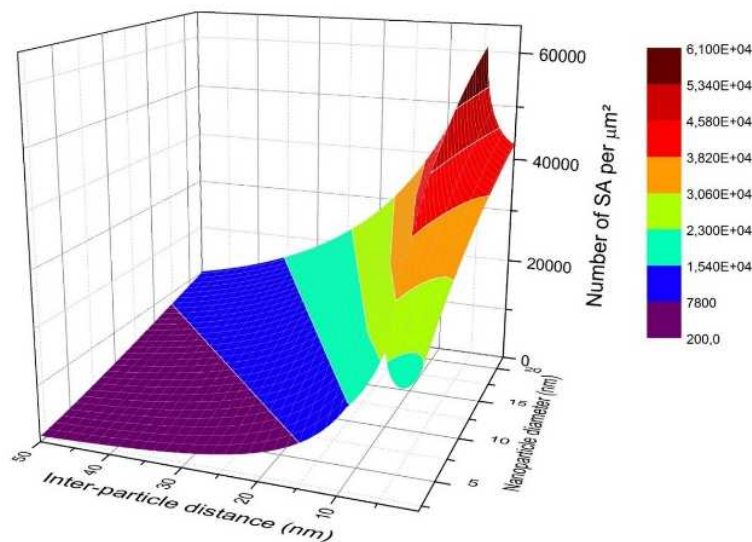


Fig. 5. Theoretical number of SA per μm^2 calculated as a function of their size and of the interparticle distance.

According to these results, we estimated the amount of SA adsorbed per surface unit onto each sample. Given the nanoparticle density measured from SEM images, we calculated the mean interparticle distances of 9.4 nm and 16.7 nm for NP6_{48h} and NP6_{8h}, respectively (see SI). These values being longer than the size of SA,^[34] it is the best configuration for SA adsorption onto the nanoparticles. It increases from 16 800 SA/ μm^2 for NP6_{8h} to 37 100 SA/ μm^2 for NP6_{48h}. Therefore, the increase of the spectral shift

from 11 to 27 nm is proportional to the number of nanoparticles, i.e. the number of available biotin groups.

In the case of NP10_{48h}, a mean interparticle distance of 6.7 nm corresponds to a maximum value of 35 125 SA/ μm^2 . This value is slightly lower than NP6_{48h} although SPR shifts are identical (27 nm). Besides the available surface of biotin groups, the effect of the larger VFe_{3- δ} O₄ of NP10_{48h} predominates on the SPR shift. Nevertheless, we would have expected a larger SPR shift according to the large increase of VFe_{3- δ} O₄ (about 4.7 times) with respect to the difference in adsorbed SA (about 5 %). It can be ascribed to the tight packing of NP10 nanoparticles, which reduces significantly the available surface of biotin at the nanoparticle surface. Indeed, dipolar interactions favor the close packing of nanoparticles during the assembly process.[35] The number of adsorbed SA onto NP10_{48h} is certainly lower than the value calculated, which explains the identical values of the SPR shift for NP6_{48h} and NP10_{48h}.

The effect of the interplay between the available surface of nanoparticles and VFe_{3- δ} O₄ on the SPR shift is also confirmed by NP22_{48h}, which displays the highest spectral shift (53 nm). Indeed, the SPR shift is 2 times larger than the one of NP10_{48h} although the available surface area for SA adsorption (42 770 SA/ μm^2) only increased by 1.2. It shows that the optical properties of iron oxide nanoparticles enhance significantly the sensitivity. Above a critical value of VFe_{3- δ} O₄, they predominate over the available surface for SA adsorption. This assumption is also supported by the arrangement of NP22, which is even more tightly packed than NP10 because of much stronger dipolar interactions.[35]

According to the calculated amount of SA adsorbed onto each sample, the maximum theoretical SPR shifts ($\Delta\lambda_{\text{th}}$) were calculated in order to compare them to experimental values. Considering the molecular weight of SA (52.1 kDa) and the mass of adsorbed SA, the theoretical effective thickness t_{th} can be determined using the Freiter equation (Table 2, see SI).[36] Then $\Delta\lambda_{\text{th}}$ was calculated according to the Campbell equation with m and l_d that were determined experimentally at specific wavelengths for a gold thin film without nanoparticles (see SI). The calculated values of $\Delta\lambda_{\text{th}}$ are much lower than the experimental data (Table 2). The difference between $\Delta\lambda_{\text{th}}$ and $\Delta\lambda$ increases from 1.2 for NP6_{8h} up to almost 2 for NP22_{48h}. These results show that m and l_d are much higher in the presence of nanoparticles than for a naked gold thin film. Therefore, the $\Delta\lambda / \Delta\lambda_{\text{th}}$ ratio can be defined as the enhancement factor of the SPR response. Plotting $\Delta\lambda / \Delta\lambda_{\text{th}}$ as a function of VFe_{3- δ} O₄ shows the non-linear increase of the enhancement ratio when the volume fraction of iron oxide increases (Fig. S7). Our system is similar to the nearly-guided wave SPR configuration described by Lahav et al.[18,20] The assembly of nanoparticles can be considered as an inhomogeneous thin layer featured by a high refractive index real part localized at the metal surface.[17] It results in the enhancement of the electromagnetic field at the gold/dielectric interface, which increases the sensitivity.

Table 2. Positions and shifts of the SPR peak after adsorption of SA onto assemblies of nanoparticles of different sizes and densities. Theoretical values of the SPR shift and of the effective thickness corresponding to the maximum amount of SA adsorbed at the nanoparticle surface.

	NP6 _{8h}	NP6 _{48h}	NP10 _{48h}	NP22 _{48h}
Peak position before SA adsorption (nm)	611	628	668	893
Spectral shift $\Delta\lambda$ after SA adsorption (nm)	11	27	27	53
Calculated number of SA per μm^2	16 800	37 100	35 100	42 800
Theoretical thickness of adsorbate layer t_{th} (nm)	1.3	2.6	2.7	3.2
Theoretical spectral shift $\Delta\lambda_{th}$ (nm)	9	16	16	28

4. Conclusion

Assemblies of iron oxide nanoparticles were prepared in order to enhance the sensitivity of the surface plasmon resonance of gold thin films prior to the detection of analytes. Nanoparticles with sizes of 6, 10 and 22 nm were synthesized by the thermal decomposition method. The CuAAC “click” reaction allowed to build robust hierarchical structures which consist in nanoparticles assemblies with biotin receptors grafted at their surface. The structure of nanoparticle assemblies was modulated by varying the density and the size of nanoparticles. The increase of the volume fraction of iron oxide at the surface of the gold thin film led to the significant shift of the SPR signal to longer wavelengths. The highest the wavelength, the largest shift of the SPR signal was observed after adsorption of streptavidine. Nevertheless, it also depends of a minimum interparticle distance that enhances the availability of biotin groups at the nanoparticle surface. We showed that the enhancement of SPR sensitivity is related to the interplay between the volume fraction of iron oxide and the amount of available biotin groups grafted at the nanoparticle surface. This study brings important information on the way the spatial arrangement of nanoparticles assembled onto a gold thin film influences the detection of analytes. Our approach is highly versatile since it can be applied for other types of nanoparticles and biomolecular receptors. Furthermore, the high tunability of the assembly structure allows setting parameters which are the most suited according to the size of various analytes. This work opens wide perspectives regarding the development of this new type of SPR sensors based on nanoparticle assemblies.

Acknowledgements

The PhD thesis of M. D. was granted by Ministère de la Recherche et de l’Enseignement Supérieur through the PhD school “Physique et Chimie Physique” (ED182) from the Université de Strasbourg. Dr.

X. Cattoën from Institut Néel (Grenoble, France) is acknowledge for providing phosphonic acid derivative for nanoparticle functionalization prior to the preparation of azido-terminated nanoparticles.

Supplementary material

The following are the Supplementary data to this article: TEM micrographs and size distribution of nanoparticles, AFM images and PM-IRRAS spectra of nanoparticle assemblies after functionalization by biotin. Theoretical calculation of the amount of SA as a function of the nanoparticle size and density.

References

- [1] R.H. Ritchie, E.T. Arakawa, J.J. Cowan, R.N. Hamm, Surface-Plasmon Resonance Effect in Grating Diffraction, (1968) 1530.
- [2] S.S. Abdulhalim I, Spectral Interrogation based SPR Sensor for Blood Glucose Detection with Improved Sensitivity and Stability, *Journal of Biosensors & Bioelectronics*. 06 (2015). <https://doi.org/10.4172/2155-6210.1000172>.
- [3] J. Homola, Surface Plasmon Resonance Sensors for Detection of Chemical and Biological Species, *Chemical Reviews*. 108 (2008) 462–493. <https://doi.org/10.1021/cr068107d>.
- [4] M. Piliarik, J. Homola, Surface plasmon resonance (SPR) sensors: approaching their limits?, *Optics Express*. 17 (2009) 16505. <https://doi.org/10.1364/OE.17.016505>.
- [5] F. Vollmer, Taking detection to the limit, *B.I.F. Futura*. 20 (2005) 6.
- [6] R. Karlsson, F. Anders, Experimental design for kinetic analysis of protein-protein interactions with surface plasmon resonance biosensors, (1997) 121–133.
- [7] J.T. Hastings, J. Guo, P.D. Keathley, P.B. Kumaresh, Y. Wei, S. Law, L.G. Bachas, Optimal self-referenced sensing using long- and short- range surface plasmons, *Optics Express*. 15 (2007) 17661. <https://doi.org/10.1364/OE.15.017661>.
- [8] J. Dostálek, J. Homola, Surface plasmon resonance sensor based on an array of diffraction gratings for highly parallelized observation of biomolecular interactions, *Sensors and Actuators B: Chemical*. 129 (2008) 303–310. <https://doi.org/10.1016/j.snb.2007.08.012>.
- [9] E.K. Popov, N. Bonod, S. Enoch, Comparison of plasmon surface waves on shallow and deep metallic 1D and 2D gratings, *Optics Express*. 15 (2007) 4224. <https://doi.org/10.1364/OE.15.004224>.
- [10] C.J. Alleyne, A.G. Kirk, R.C. McPhedran, N.-A.P. Nicorovici, D. Maystre, Enhanced SPR sensitivity using periodic metallic structures, *Optics Express*. 15 (2007) 8163. <https://doi.org/10.1364/OE.15.008163>.
- [11] S.Y. Wu, H.P. Ho, W.C. Law, C. Lin, S.K. Kong, Highly sensitive differential phase-sensitive surface plasmon resonance biosensor based on the Mach–Zehnder configuration, *Optics Letters*. 29 (2004) 2378. <https://doi.org/10.1364/OL.29.002378>.
- [12] Y.-D. Su, S.-J. Chen, T.-L. Yeh, Common-path phase-shift interferometry surface plasmon resonance imaging system, *Optics Letters*. 30 (2005) 1488. <https://doi.org/10.1364/OL.30.001488>.
- [13] J.-Y. Lee, T.-K. Chou, H.-C. Shih, Polarization-interferometric surface-plasmon-resonance imaging system, *Optics Letters*. 33 (2008) 434. <https://doi.org/10.1364/OL.33.000434>.
- [14] S. Zeng, X. Yu, W.-C. Law, Y. Zhang, R. Hu, X.-Q. Dinh, H.-P. Ho, K.-T. Yong, Size dependence of Au NP-enhanced surface plasmon resonance based on differential phase measurement, *Sensors and Actuators B: Chemical*. 176 (2013) 1128–1133. <https://doi.org/10.1016/j.snb.2012.09.073>.
- [15] A. Shalabney, I. Abdulhalim, Electromagnetic fields distribution in multilayer thin film structures and the origin of sensitivity enhancement in surface plasmon resonance sensors, *Sensors and Actuators A: Physical*. 159 (2010) 24–32. <https://doi.org/10.1016/j.sna.2010.02.005>.
- [16] S. Szunerits, A. Shalabney, R. Boukherroub, I. Abdulhalim, Dielectric coated plasmonic interfaces: their interest for sensitive sensing of analyte-ligand interactions, *Reviews in Analytical Chemistry*. 31 (2012). <https://doi.org/10.1515/revac.2011.120>.
- [17] A. Shalabney, C. Khare, B. Rauschenbach, I. Abdulhalim, Sensitivity of surface plasmon resonance sensors based on metallic columnar thin films in the spectral and angular interrogations, *Sensors and Actuators B: Chemical*. 159 (2011) 201–212. <https://doi.org/10.1016/j.snb.2011.06.072>.
- [18] A. Lahav, Surface plasmon sensor with enhanced sensitivity using top nano dielectric layer, *Journal of Nanophotonics*. 3 (2009) 031501. <https://doi.org/10.1117/1.3079803>.

- [19] A. Shalabney, A. Lakhtakia, I. Abdulhalim, A. Lahav, C. Patzig, I. Hazeq, A. Karabchevsky, B. Rauschenbach, F. Zhang, J. Xu, Surface plasmon resonance from metallic columnar thin films, *Photonics and Nanostructures - Fundamentals and Applications*. 7 (2009) 176–185. <https://doi.org/10.1016/j.photonics.2009.03.003>.
- [20] A. Lahav, M. Auslender, I. Abdulhalim, Sensitivity enhancement of guided-wave surface-plasmon resonance sensors, *Optics Letters*. 33 (2008) 2539. <https://doi.org/10.1364/OL.33.002539>.
- [21] S. Szunerits, R. Boukherroub, Preparation and Characterization of Thin Films of SiO_x on Gold Substrates for Surface Plasmon Resonance Studies, *Langmuir*. 22 (2006) 1660–1663. <https://doi.org/10.1021/la052773c>.
- [22] J. Ryken, J. Li, T. Steylaerts, R. Vos, J. Loo, K. Jans, W. Van Roy, T. Stakenborg, P. Van Dorpe, J. Lammertyn, L. Lagae, Biosensing with SiO₂-covered SPR substrates in a commercial SPR-tool, *Sensors and Actuators B: Chemical*. 200 (2014) 167–172. <https://doi.org/10.1016/j.snb.2014.04.060>.
- [23] Y.-S. Choi, C. Won Yoon, H. Dong Lee, M. Park, J. Won Park, Efficient protein–ligand interaction by guaranteeing mesospacing between immobilized biotins, *Chem. Commun.* (2004) 1316–1317. <https://doi.org/10.1039/B403797A>.
- [24] B.P. Pichon, G. Barbillon, P. Marie, M. Pauly, Sylvie. Begin-Colin, Iron oxide magnetic nanoparticles used as probing agents to study the nanostructure of mixed self-assembled monolayers., *Nanoscale*. 3 (2011) 4696–4705. <https://doi.org/10.1039/c1nr10729a>.
- [25] N.S. Lynn, J. Homola, (Bio)Sensing Using Nanoparticle Arrays: On the Effect of Analyte Transport on Sensitivity, *Anal. Chem.* 88 (2016) 12145–12151. <https://doi.org/10.1021/acs.analchem.6b03002>.
- [26] M. Dolci, J.-F. Bryche, C. Leuvrey, S. Zafeiratos, S. Gree, S. Begin-Colin, G. Barbillon, B.P. Pichon, Robust clicked assembly based on iron oxide nanoparticles for a new type of SPR biosensor, *Journal of Materials Chemistry C*. 6 (2018) 9102–9110. <https://doi.org/10.1039/C8TC01166D>.
- [27] Y. Cao, E. Galoppini, P.I. Reyes, Y. Lu, Functionalization of Nanostructured ZnO Films by Copper-Free Click Reaction, *Langmuir*. 29 (2013) 7768–7775. <https://doi.org/10.1021/la4006949>.
- [28] D. Toulemon, B.P. Pichon, X. Cattoen, M.W.C. Man, S. Begin-Colin, 2D assembly of non-interacting magnetic iron oxide nanoparticles via “click” chemistry, *Chemical Communications*. 47 (2011). <http://dx.doi.org/10.1039/C1CC14661K>.
- [29] W. Baaziz, B.P. Pichon, S. Fleutot, Y. Liu, C. Lefevre, J.-M. Greneche, M. Toumi, T. Mhiri, S. Begin-Colin, Magnetic Iron Oxide Nanoparticles: Reproducible Tuning of the Size and Nanosized-Dependent Composition, Defects, and Spin Canting, *The Journal of Physical Chemistry C*. 118 (2014) 3795–3810. <https://doi.org/10.1021/jp411481p>.
- [30] D. Toulemon, B.P. Pichon, X. Cattoen, M.W. Man, S. Begin-Colin, 2D assembly of non-interacting magnetic iron oxide nanoparticles via "click" chemistry, *Chem Commun (Camb)*. 47 (2011) 11954–6. <https://doi.org/10.1039/c1cc14661k>.
- [31] M. Dolci, Y. Lei, L.-M. Lacroix, C. Kiefer, C. Leuvrey, S. Begin-Colin, B.P. Pichon, Effect of Dipolar Interactions on the Assembly Process of Iron Oxide Nanoparticles Promoted by the CuAAC “Click” Chemistry Reaction, *J. Phys. Chem. C*. 123 (2019) 27927–27936. <https://doi.org/10.1021/acs.jpcc.9b08135>.
- [32] N.A. Lapin, Y.J. Chabal, Infrared characterization of biotinylated silicon oxide surfaces, surface stability, and specific attachment of streptavidin, *The Journal of Physical Chemistry. B*. 113 (2009) 8776–83. <https://doi.org/10.1021/jp809096m>.
- [33] C.T.C. Linda S. Jung Timothy M. Chinowsky, Mimi N. Mar, and Sinclair S. Yee, Quantitative Interpretation of the Response of Surface Plasmon Resonance Sensors to Adsorbed Films, *Langmuir*. 14 (1998) 5636–5648.

- [34] R.C.S. Scott D. Soelberg Ajit P. Limaye, and Clement E. Furlong, Surface Plasmon Resonance Detection Using Antibody-Linked Magnetic Nanoparticles for Analyte Capture, Purification, Concentration, and Signal Amplification, *Anal Chem.* 81 (2009) 2357–2363.
- [35] Dolci, Mathias, Lei, Yu-ting, Lacroix, Lise Marie, Kiefer, Céline, Leuvrey, Cédric, Begin-Colin, Sylvie, Pichon, Benoit P., Effect of dipolar interactions on the assembly process of iron oxide nanoparticles promoted by the CuAAC « click » chemistry reaction, (2019) submitted.
- [36] W.M. Albers, I. Vikholm-Lundin, Surface Plasmon Resonance on Nanoscale Organic Films, in: *Nano-Bio-Sensing*, Springer, New York, NY, 2011: pp. 83–125. https://doi.org/10.1007/978-1-4419-6169-3_4.

